

# Graph Canonical Coherence Analysis

KYUSOON KIM<sup>1</sup> AND HEE-SEOK OH<sup>2\*</sup>

<sup>1</sup>Department of Statistics and Actuarial Science, Soongsil University, Seoul 06978, Korea

<sup>2</sup>Department of Statistics, Seoul National University, Seoul 08826, Korea

## Abstract

We propose graph canonical coherence analysis (gCChA), a novel framework that extends canonical correlation analysis to multivariate graph signals in the graph frequency domain. The proposed method addresses challenges posed by the inherent features of graphs: discreteness, finiteness, and irregularity. It identifies pairs of canonical graph signals that maximize their coherence, enabling the exploration of relationships between two sets of graph signals from a spectral perspective. This framework shows how these relationships change across different structural scales of the graph. We demonstrate the usefulness of this method through applications to economic and energy datasets of G20 countries and the USPS handwritten digit dataset.

**Keywords:** Canonical correlation analysis; Dimension reduction; Frequency domain; Graph signal processing; Multivariate graph signal.

## 1 Introduction

Canonical correlation analysis (CCA), originally proposed by Hotelling (1935, 1936), is a classical multivariate method for quantifying a linear relationship between two sets of multidimensional variables. This method finds pairs of canonical components, which are linear combinations of variables from each set that achieve the highest possible correlation. Through these components, CCA summarizes the dependence structure between the two

---

\*Corresponding author: heeseok@stats.snu.ac.kr

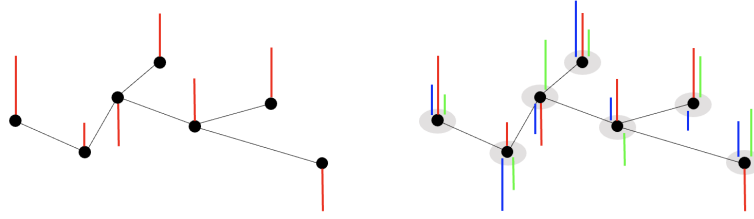


Figure 1: Illustration of univariate (left) and multivariate (right) graph signals.

sets in a lower-dimensional space. In this regard, it can be viewed as a dimension reduction method that extends the concept of principal component analysis (PCA) to two sets of variables. Thus, CCA is often used to evaluate both the strength and the underlying structure of relationships between the two sets. It has been applied in a wide range of fields, including neuroscience (Mihalik et al., 2022; Zhuang et al., 2020), bioinformatics (Cichonska et al., 2016; Wróbel et al., 2024), finance (Mazuruse, 2014), and deep learning (Andrew et al., 2013; Yang et al., 2017), in tasks such as blind source separation, clustering, and classification. For a comprehensive overview of CCA, refer to Yang et al. (2019), Uurtio et al. (2017), Kuylen and Verhallen (1981), Thompson (1984), Johnson and Wichern (2007), and Hardoon et al. (2004).

Classical CCA deals with multidimensional data in Euclidean space, where each set of variables corresponds to a vector. Brillinger (2001) further extended CCA to analyze two multivariate time series by formulating it in the frequency domain. However, in many fields, data are observed on irregular domains characterized by graph structures, known as graph signals (Leus et al., 2023; Ortega et al., 2018; Shuman et al., 2013), highlighting the need to develop CCA tailored for such domains. Specifically, univariate graph signals are scalar values located on the nodes (or vertices) of a graph, while multivariate graph signals consist of vector-valued data associated with each node, as shown in Figure 1. In the figure, the height and direction (upward or downward) of each bar indicate the magnitude and sign of the signal value mapped to each node, and bars with the same color represent values corresponding to the same attribute in the multivariate case. Graph signals defined on a path or cycle graph can be viewed as special cases that correspond to time series.

Developing CCA for multivariate graph signals presents unique challenges due to the inherent discreteness, finiteness, and irregularity of graphs. In this study, we propose a new CCA framework for graph signals called *graph canonical coherence analysis (gCChA)*. This framework aims to discover relationships between two multivariate graph signals defined on a common underlying graph. To account for the distinctive characteristics of the graph domain, we are motivated by the frequency-domain approach of Brillinger (2001) and develop the framework in the graph frequency domain, where this frequency-domain perspective connects the time-domain and graph-domain analyses. Unlike several previous works that operate in the vertex domain, the proposed framework provides a systematic way to describe the relationships between two multivariate graph signals using low-dimensional canonical graph signals and to analyze these relationships from a spectral perspective across graph frequencies.

The rest of this paper is organized as follows. Section 2 reviews the fundamentals of graph signal processing and related work. The proposed graph canonical coherence analysis framework is presented in Section 3. Numerical experiments on economic and energy datasets from G20 countries and the US Postal Service (USPS) handwritten digit dataset are provided in Section 4. Section 5 concludes the paper with concluding remarks. The R codes are available at <https://github.com/qsoon/gCChA>.

## 2 Background

### 2.1 Graph Signals and Graph Frequency Domain

Let  $\mathcal{G} = (\mathcal{V}, \mathcal{E}, \mathcal{W})$  denote a weighted graph, possibly directed, where  $\mathcal{V}$  is the set of nodes with size  $n$ ,  $\mathcal{E}$  is the set of edges, and  $\mathcal{W}$  is the weighted adjacency matrix. In this paper, it is assumed that  $\mathcal{G}$  is finite, connected, and simple, meaning it has no self-loops or multiple edges. The nonnegative element  $w_{ij}$  of  $\mathcal{W}$  represents the weight of the edge between vertices  $i$  and  $j$ , and a value of  $w_{ij} = 0$  indicates no direct connection between them. A graph signal assigns a scalar or vector value to each node of  $\mathcal{G}$ . A univariate graph signal can be viewed as a function  $x : \mathcal{V} \rightarrow \mathbb{R}$  (or  $\mathbb{C}$ ), while a multivariate graph signal extends this to higher-dimensional codomains. In the univariate case, the signal is

represented by a vector  $x$  of size  $n$ , whose  $i$ th entry corresponds to the value at node  $i$ .

A key concept in graph signal processing (GSP) is the graph shift operator (GSO), denoted by  $S$ , which defines local interactions between neighboring vertices. Multiplying  $S$  by a univariate signal  $x \in \mathbb{R}^n$  (or  $\mathbb{C}^n$ ) generates a new signal whose value at each vertex is a weighted sum of the signal values at its neighbors (Sandryhaila and Moura, 2013; Segarra et al., 2018). Common choices for GSOs include the weighted adjacency matrix and the graph Laplacian. For an undirected graph, the Laplacian is defined as  $L = \text{diag}(\{\sum_{j=1}^n w_{ij}\}_{i=1}^n) - W$ , where  $w_{ij}$  denotes the  $(i, j)$ th element of the weighted adjacency matrix  $W$ .

The graph Laplacian  $L$  is symmetric and positive semidefinite, and its quadratic form  $x^\top L x = \frac{1}{2} \sum_{i=1}^n \sum_{j=1}^n w_{ij} (x_i - x_j)^2$  quantifies the total variation, or smoothness, of  $x$  over the graph. Since  $L$  admits the eigendecomposition  $L = V \Lambda V^\top$ , where  $V = (v_1 \mid \dots \mid v_n)$  contains orthonormal eigenvectors and  $\Lambda = \text{diag}(\lambda_1, \dots, \lambda_n)$  with  $0 = \lambda_1 < \lambda_2 \leq \dots \leq \lambda_n$ , the eigenvalue  $\lambda_i$  can be interpreted as the graph frequency corresponding to the basis vector  $v_i$ . From the perspective of total variation measured by the quadratic form of the graph Laplacian  $L$ , the total variation of  $v_i$  is expressed as  $v_i^\top L v_i = \lambda_i$ . Therefore,  $v_1$  shows the smallest total variation, making  $\lambda_1$  the lowest graph frequency, while  $v_n$  exhibits the largest total variation, making  $\lambda_n$  the highest graph frequency. In particular, the first eigenvector  $v_1 \propto (1, \dots, 1)^\top$  is constant across nodes, representing the smoothest mode.

In more general settings, the GSO  $S$  is assumed to be normal, allowing it to be decomposed as  $S = V \Lambda V^H$ , where  $V$  is unitary and  $\Lambda$  is diagonal with eigenvalues  $\lambda_1, \dots, \lambda_n$ . For such operators, the concept of frequency ordering can be established using the total variation of eigenvectors. Following Sandryhaila and Moura (2014) and Singh et al. (2016), eigenvectors with smaller total variation are considered low-frequency components, while those with larger variation are regarded as high-frequency components. The total variation of  $x$  may be defined, for example, through the discrete  $p$ -Dirichlet form  $\frac{1}{p} \|x - Sx\|_p^p$ , where  $\|\cdot\|_p$  denotes the  $L_p$  norm. In the case of a unitary shift operator and  $p = 2$ , the total variation of the eigenvector  $v_i$  becomes  $\frac{1}{2} \|(1 - \lambda_i)v_i\|_2^2$ , and the frequencies are ordered according to  $|1 - \lambda_i|$ .

Given the eigendecomposition  $S = V \Lambda V^H$  with eigenvalues ordered from low to high

frequencies, the graph Fourier transform (GFT) of a signal  $x$  is defined as  $V^H x$ , where each element represents a spectral coefficient at a specific graph frequency. GFT thus transforms a signal from the vertex domain into the graph frequency (or spectral) domain, similar to the classical Fourier transform.

A linear and shift-invariant (LSI) graph filter is a linear operator that modifies graph spectral components in a frequency-dependent manner. It can be written as  $H = \sum_{\ell=1}^n h_\ell S^{\ell-1} = V \text{diag}(\{h(\lambda_\ell)\}_{\ell=1}^n) V^H$ , where  $h(\lambda) = \sum_{\ell=1}^n h_\ell \lambda^{\ell-1}$  denotes the frequency response of the filter (Sandryhaila and Moura, 2013). The filtered output of  $x$  is then  $Hx$ . These filters are essential in GSP for tasks like denoising, smoothing, and signal reconstruction on graphs (Tremblay et al., 2018). In this paper, the term ‘graph filter’ specifically refers to LSI graph filters unless stated otherwise.

## 2.2 Stationarity and Spectral Densities on Graphs

The concept of weak stationarity for random processes on graphs has been widely used in statistical graph signal processing (Girault, 2015; Kim and Oh, 2024, 2025a; Marques et al., 2017; Perraudin and Vanderghenst, 2017). The definition of weak stationarity for multivariate random graph processes below was introduced by Kim and Oh (2024) as an extension of the univariate notion in Marques et al. (2017).

**Definition 2.1.** (Kim and Oh, 2024) Given a normal graph shift operator  $S$ , consider a zero-mean  $p$ -dimensional random graph process  $X = (X_1 \mid \dots \mid X_p)$ , where each  $X_i$  ( $1 \leq i \leq p$ ) is an  $n$ -dimensional vector. The random graph process  $X$  is said to be weakly stationary if the cross-covariance matrices  $\Sigma_{ij}^X := \text{Cov}(X_i, X_j)$  and  $S$  are simultaneously diagonalizable for  $1 \leq i, j \leq p$ .

If  $X_i$  ( $1 \leq i \leq p$ ) are not zero-mean random graph processes, their first moments are required to satisfy  $\mathbb{E}[X_i] \propto v_j$  ( $1 \leq j \leq n$ ).

For a weakly stationary random graph process  $X$ , Kim and Oh (2025a) defined the graph cross-spectral density (GCSD) between  $X_i$  and  $X_j$  ( $1 \leq i, j \leq p$ ) as an  $n \times 1$  vector

$$p_{ij}^X = (p_{ij}^X(\lambda_1), \dots, p_{ij}^X(\lambda_n))^\top = \text{diag}(V^H \Sigma_{ij}^X V).$$

GCSD characterizes the frequency-wise dependence between two graph signals. When  $i = j$ , this becomes the graph power spectral density (GPSD) of  $X_i$  introduced in Marques et al. (2017), which shows the distribution of signal energy across graph frequencies. Both GPSD and GCSD can be estimated using the windowed average graph periodogram and graph cross-periodogram, respectively, with random windows applicable in practical implementations (Kim and Oh, 2025a). The (squared) graph coherence between  $X_i$  and  $X_j$  ( $1 \leq i, j \leq p$ ) was subsequently defined in Kim and Oh (2025a), as follows.

**Definition 2.2.** (Kim and Oh, 2025a) Let  $X = (X_1 | \cdots | X_p)$  be a weakly stationary, zero-mean,  $p$ -dimensional random graph process. The (squared) graph coherence between  $X_i$  and  $X_j$ ,  $c_{ij}^X = (c_{ij}^X(\lambda_1), \dots, c_{ij}^X(\lambda_n))^\top$ , is defined as

$$c_{ij}^X(\lambda_\ell) = \frac{|p_{ij}^X(\lambda_\ell)|^2}{p_{ii}^X(\lambda_\ell) p_{jj}^X(\lambda_\ell)}, \quad 1 \leq i, j \leq p, 1 \leq \ell \leq n.$$

For brevity, ‘weak stationarity’ will hereafter be called ‘stationarity,’ and ‘(squared) graph coherence’ as ‘graph coherence.’ The term ‘graph signal’ is also used interchangeably to refer to either a random graph process or its realization, depending on the context.

### 2.3 Related Work

Several studies have integrated graph structures into CCA. Yuan and Sun (2014) proposed a graph-regularized multiset canonical correlation analysis method, termed GrMCCA. They consider multiple datasets, with the  $i$ th dataset having  $p_i$  variables measured on the same  $n$  observations across multiple classes. For each dataset, they build two  $k$ -nearest-neighbor graphs based on cosine similarities between observations: a within-class graph  $\mathcal{G}_w^{(i)}$  using neighbors from the same class, which captures the local geometry of within-class data points, and a between-class graph  $\mathcal{G}_b^{(i)}$  using neighbors from different classes, reflecting the local geometry of between-class data points. The local intraclass scatter is measured as the smoothness of the canonical variable  $\alpha^{(i)}$  on  $\mathcal{G}_w^{(i)}$ , computed by  $(\alpha^{(i)})^\top L_w^{(i)} \alpha^{(i)}$ , where  $L_w^{(i)}$  is its graph Laplacian. Similarly, the interclass scatter is defined using  $(\alpha^{(i)})^\top L_b^{(i)} \alpha^{(i)}$ . GrMCCA maximizes correlations between canonical variables while minimizing total intraclass scatter and maximizing interclass scatter.

Chen et al. (2018) proposed a graph-regularized CCA method, called gCCA. This approach assumes the existence of low-dimensional common latent sources that generate the two datasets, aligning with the perspective of Bach and Jordan (2005). It also assumes the inherent geometric structure of the common sources encoded in a graph  $\mathcal{G}_s$ . This source graph can be provided or constructed based on prior knowledge, and its nodes represent the  $n$  observations. Consequently, the common sources of the  $n$  observations can be viewed as a multivariate graph signal on  $\mathcal{G}_s$ ,  $s = (s_1, \dots, s_n)^\top$ , where  $s_i \in \mathbb{R}^\rho$ . This method further assumes that this graph signal is smooth. This assumption, together with the fact that the canonical variables  $\alpha_i$  and  $\beta_j$  serve as one-dimensional approximations of  $s_i$  and  $s_j$ , leads to determining the canonical variables  $\alpha = (\alpha_1, \dots, \alpha_n)^\top$  and  $\beta = (\beta_1, \dots, \beta_n)^\top$  by maximizing  $\text{Corr}(\alpha, \beta) - \gamma \alpha^\top L_s \beta$ , where  $L_s$  denotes the graph Laplacian of  $\mathcal{G}_s$ . Chen et al. (2019) further extended gCCA to multiview settings, resulting in MGCCA. These methods operate in the vertex domain and impose smoothness constraints on the canonical variables. While this assumption is often valid, it does not always apply. Additionally, these methods do not explicitly address the interpretability of the resulting canonical variables: although the solutions are affected by graph regularization, it is difficult to understand them in terms of the underlying graph structure.

In contrast, the proposed method incorporates the graph structure in the frequency domain, providing a more general framework beyond cases in which canonical variables on neighboring nodes are expected to have similar values. Importantly, it produces interpretable canonical variables through a multiscale spectral perspective, offering insights unavailable in existing node-domain approaches. We compare the proposed method with gCCA by Chen et al. (2018) via an image classification task in Section 4.2, as gCCA is the most relevant baseline.

We further note a recent paper of Park et al. (2025). This paper introduces a graph CCA method to address the limitation of conventional CCA, which often fails to incorporate structured patterns in the cross-correlation matrix between two sets of variables. However, their approach fundamentally differs from the previous works mentioned above and from our method because it uses a bipartite graph in which the nodes represent the variables of the two datasets, rather than a graph structure based on observations.

### 3 Proposed Method

#### 3.1 Graph Canonical Coherence Analysis and Its Properties

Let  $X = (X_1 | \cdots | X_p)$  and  $Y = (Y_1 | \cdots | Y_q)$  denote  $p$ -dimensional and  $q$ -dimensional graph signals on a graph  $\mathcal{G}$ , respectively. We first construct an  $r$ -dimensional graph signal  $Z = (Z_1 | \cdots | Z_r)$  for  $r \leq \min(p, q)$ , where each component is defined as a sum of graph-filtered outputs of signals  $X_1, \dots, X_p$ ,

$$Z_i = H_{i1}X_1 + \cdots + H_{ip}X_p =: \mathcal{T}_i^H(X), \quad 1 \leq i \leq r. \quad (1)$$

Here,  $H_{ij} = V \text{diag}(\{h_{ij}(\lambda_\ell)\}_{\ell=1}^n) V^H$  is a graph filter, and  $\mathcal{T}_i^{(\cdot)}(\cdot)$  denotes a linear operator that sums graph-filtered outputs. Next, we seek to approximate  $Y_i$  using a sum of graph-filtered outputs of  $Z_1, \dots, Z_r$ ,

$$\mu_i + G_{i1}Z_1 + \cdots + G_{ir}Z_r =: \mu_i + \mathcal{T}_i^G(Z), \quad 1 \leq i \leq q, \quad (2)$$

where  $\mu_i$  is a vector of length  $n$  and  $G_{ij} = V \text{diag}(\{g_{ij}(\lambda_\ell)\}_{\ell=1}^n) V^H$  is a graph filter. Substituting the expression of  $Z_i$  in (1) into (2), we obtain

$$\mu_i + A_{i1}X_1 + \cdots + A_{ip}X_p =: \mu_i + \mathcal{T}_i^A(X), \quad 1 \leq i \leq q,$$

where  $A_{ij} = G_{i1}H_{1j} + \cdots + G_{ir}H_{rj}$  is a graph filter with frequency responses  $a_{ij}(\lambda_\ell) = g_{i1}(\lambda_\ell)h_{1j}(\lambda_\ell) + \cdots + g_{ir}(\lambda_\ell)h_{rj}(\lambda_\ell)$ , i.e.,  $A_{ij} = V \text{diag}(\{a_{ij}(\lambda_\ell)\}_{\ell=1}^n) V^H$ . We aim to minimize the mean squared error  $\sum_{i=1}^q E[(Y_i - (\mu_i + \mathcal{T}_i^A(X)))^H(Y_i - (\mu_i + \mathcal{T}_i^A(X)))]$ , where the solution is given by the following theorem.

**Theorem 3.1.** *Let  $XY = (X_1 | \cdots | X_p | Y_1 | \cdots | Y_q)$  be a  $(p+q)$ -dimensional stationary graph signal with respect to the graph shift operator  $S = V\Lambda V^H$  on  $\mathcal{G}$ . The means of  $X_i$  and  $Y_j$  are denoted by  $\mu_i^X$  and  $\mu_j^Y$ , respectively. Let  $p_{ij}^X$  and  $p_{ij}^Y$  denote the graph cross-spectral densities of  $(X_i, X_j)$  and  $(Y_i, Y_j)$ , respectively, and let  $p_{ij}^{XY}$  and  $p_{ij}^{YX}$  denote the graph cross-spectral densities of  $(X_i, Y_j)$  and  $(Y_i, X_j)$ , respectively. For each graph frequency  $\lambda_\ell$  ( $1 \leq \ell \leq n$ ), define the spectral matrices*

$$P_X(\lambda_\ell) \in \mathbb{C}^{p \times p}, \quad P_Y(\lambda_\ell) \in \mathbb{C}^{q \times q}, \quad P_{XY}(\lambda_\ell) \in \mathbb{C}^{p \times q}, \quad P_{YX}(\lambda_\ell) \in \mathbb{C}^{q \times p},$$

whose  $(i, j)$ th elements are  $p_{ij}^X(\lambda_\ell)$ ,  $p_{ij}^Y(\lambda_\ell)$ ,  $p_{ij}^{XY}(\lambda_\ell)$ , and  $p_{ij}^{YX}(\lambda_\ell)$ , respectively. Suppose that  $P_X(\lambda_\ell)$  and  $P_Y(\lambda_\ell)$  are nonsingular for all  $1 \leq \ell \leq n$ . Then,  $\{\mu_i\}_{i=1}^q$  and  $\{A_{ij}\}_{1 \leq i \leq q, 1 \leq j \leq p}$  that minimize the mean squared error  $\sum_{i=1}^q E[(Y_i - (\mu_i + \mathcal{T}_i^A(X)))^H(Y_i - (\mu_i + \mathcal{T}_i^A(X)))]$ , are given by

$$\mu_i = \mu_i^Y - \sum_{j=1}^r G_{ij} \left( \sum_{k=1}^p H_{jk} \mu_k^X \right) \quad \text{and} \quad A(\lambda_\ell) = G(\lambda_\ell) H(\lambda_\ell),$$

where  $H(\lambda_\ell) = (u_1(\lambda_\ell) | \cdots | u_r(\lambda_\ell))^H P_{YX}(\lambda_\ell) P_X(\lambda_\ell)^{-1}$  and  $G(\lambda_\ell) = (u_1(\lambda_\ell) | \cdots | u_r(\lambda_\ell))$ . Here, the matrices  $A(\lambda_\ell)$ ,  $H(\lambda_\ell)$ , and  $G(\lambda_\ell)$  are of size  $q \times p$ ,  $r \times p$ , and  $q \times r$ , respectively, and their  $(i, j)$ th elements are  $a_{ij}(\lambda_\ell)$ ,  $h_{ij}(\lambda_\ell)$ , and  $g_{ij}(\lambda_\ell)$ . Also  $u_i(\lambda_\ell)$  denotes the  $i$ th orthonormal eigenvector of  $P_{YX}(\lambda_\ell) P_X(\lambda_\ell)^{-1} P_{XY}(\lambda_\ell)$  associated with the  $i$ th eigenvalue  $\tau_i(\lambda_\ell)$  (with  $\tau_1(\lambda_\ell) \geq \cdots \geq \tau_q(\lambda_\ell) \geq 0$ ). The minimum mean squared error is obtained as  $\sum_{\ell=1}^n \text{tr}[P_Y(\lambda_\ell) - P_{YX}(\lambda_\ell) P_X(\lambda_\ell)^{-1} P_{XY}(\lambda_\ell)] + \sum_{\ell=1}^n \sum_{i>r} \tau_i(\lambda_\ell)$ .

*Proof.* A proof is provided in Appendix A. □

If  $X = Y$ , we obtain PCA results discussed in Kim and Oh (2024).

The above approach minimizes  $\sum_{i=1}^q E[\epsilon_i^H \epsilon_i] = \sum_{\ell=1}^n \text{tr}[P_\epsilon(\lambda_\ell)]$ , where  $\epsilon = (\epsilon_1 | \cdots | \epsilon_q)$  is a  $q$ -dimensional error signal with  $\epsilon_i = Y_i - (\mu_i + \mathcal{T}_i^A(X))$ , and  $P_\epsilon(\lambda_\ell)$  denotes the spectral matrix of  $\epsilon$  at graph frequency  $\lambda_\ell$ . This criterion assigns equal weight to error values across all nodes, which may be inappropriate when signal variances vary across nodes. As an alternative, we may consider minimizing

$$\sum_{\ell=1}^n \text{tr}[P_Y(\lambda_\ell)^{-1/2} P_\epsilon(\lambda_\ell) P_Y(\lambda_\ell)^{-1/2}], \quad (3)$$

which leads to the solution stated in Corollary 3.1.

**Corollary 3.1.** *Under the conditions of Theorem 3.1, the solution minimizing (3) is determined by the eigenvectors of  $P_Y(\lambda_\ell)^{-1/2} P_{YX}(\lambda_\ell) P_X(\lambda_\ell)^{-1} P_{XY}(\lambda_\ell) P_Y(\lambda_\ell)^{-1/2}$ .*

To treat the two signals, we consider the following problem. We construct an  $r$ -dimensional graph signal  $W = (W_1 | \cdots | W_r)$ , whose components are defined as sums of graph-filtered versions of  $Y_1, \dots, Y_q$ ,

$$W_i = F_{i1} Y_1 + \cdots + F_{iq} Y_q =: \mathcal{T}_i^F(Y), \quad 1 \leq i \leq r, \quad (4)$$

where  $\mathbf{F}_{ij} = V \text{diag}(\{f_{ij}(\lambda_\ell)\}_{\ell=1}^n) V^H$  is a graph filter. The parameters are then determined by minimizing  $\sum_{i=1}^r E[(W_i - \mu_i - Z_i)^H (W_i - \mu_i - Z_i)]$  subject to the constraints  $F(\lambda_\ell)P_Y(\lambda_\ell)F(\lambda_\ell)^H = I_r$  and  $H(\lambda_\ell)P_X(\lambda_\ell)H(\lambda_\ell)^H = I_r$ , where  $H(\lambda_\ell)$  and  $F(\lambda_\ell)$  are  $r \times p$  and  $r \times q$  matrices whose  $(i, j)$ th elements are  $h_{ij}(\lambda_\ell)$  and  $f_{ij}(\lambda_\ell)$ , respectively. The corresponding solution is given in Theorem 3.2.

**Theorem 3.2.** *Under the conditions of Theorem 3.1, the solutions minimizing  $\sum_{i=1}^r E[(W_i - \mu_i - Z_i)^H (W_i - \mu_i - Z_i)]$  subject to  $F(\lambda_\ell)P_Y(\lambda_\ell)F(\lambda_\ell)^H = I_r$  and  $H(\lambda_\ell)P_X(\lambda_\ell)H(\lambda_\ell)^H = I_r$  are given by*

$$\begin{aligned}\mu_i &= \sum_{j=1}^q \mathbf{F}_{ij} \mu_j^Y - \sum_{j=1}^p \mathbf{H}_{ij} \mu_j^X, \quad 1 \leq i \leq r, \\ H(\lambda_\ell) &= (d_1(\lambda_\ell) | \cdots | d_r(\lambda_\ell))^H P_X(\lambda_\ell)^{-1/2}, \\ F(\lambda_\ell) &= (e_1(\lambda_\ell) | \cdots | e_r(\lambda_\ell))^H P_Y(\lambda_\ell)^{-1/2},\end{aligned}$$

where the matrices  $H(\lambda_\ell)$  and  $F(\lambda_\ell)$  are of sizes  $r \times p$  and  $r \times q$ , respectively, and their  $(i, j)$ th elements are  $h_{ij}(\lambda_\ell)$  and  $f_{ij}(\lambda_\ell)$ . Here,  $d_i(\lambda_\ell)$  is the  $i$ th orthonormal eigenvector of  $P_X(\lambda_\ell)^{-1/2} P_{XY}(\lambda_\ell) P_Y(\lambda_\ell)^{-1} P_{YX}(\lambda_\ell) P_X(\lambda_\ell)^{-1/2}$  and  $e_i(\lambda_\ell)$  is the  $i$ th orthonormal eigenvector of  $P_Y(\lambda_\ell)^{-1/2} P_{YX}(\lambda_\ell) P_X(\lambda_\ell)^{-1} P_{XY}(\lambda_\ell) P_Y(\lambda_\ell)^{-1/2}$ . These two matrices share the same eigenvalues, and  $d_i(\lambda_\ell)$  and  $e_i(\lambda_\ell)$  correspond to their common  $i$ th largest eigenvalue.

*Proof.* A proof is provided in Appendix A. □

Let  $h_i(\lambda_\ell) = (h_{i1}(\lambda_\ell), \dots, h_{ip}(\lambda_\ell))^H$  and  $f_i(\lambda_\ell) = (f_{i1}(\lambda_\ell), \dots, f_{iq}(\lambda_\ell))^H$ . The solutions in Theorem 3.2 can also be obtained via an alternative method. Specifically, we may sequentially find  $Z_i$  and  $W_i$  with  $h_i(\lambda_\ell)^H P_X(\lambda_\ell) h_i(\lambda_\ell) = 1$  and  $f_i(\lambda_\ell)^H P_Y(\lambda_\ell) f_i(\lambda_\ell) = 1$  for all  $1 \leq \ell \leq n$ , ensuring that the graph power spectral densities of  $Z_i$  and  $W_i$  are equal to 1 across all graph frequencies, while simultaneously maximizing the graph coherence between  $Z_i$  and  $W_i$  at each graph frequency. Additionally,  $Z_i$  and  $W_i$  are constrained to have zero coherence with  $Z_j$  and  $W_j$  for  $j = 1, \dots, i-1$  across all graph frequencies. The resulting  $Z_i$  and  $W_i$  are described in Theorem 3.3 and are equivalent to the solutions in Theorem 3.2.

**Theorem 3.3.** *Assume the conditions of Theorem 3.1. The solutions maximizing the graph coherence of  $Z_i$  and  $W_i$  across each graph frequency, subject to the constraints that (i) the graph power spectral densities of  $Z_i$  and  $W_i$  are equal to 1 across all frequencies, and (ii)  $Z_i$  and  $W_i$  have zero coherence with  $Z_j$  and  $W_j$  for  $j = 1, \dots, i-1$  across all graph frequencies, are given by*

$$h_i(\lambda_\ell) \propto P_X(\lambda_\ell)^{-1} P_{XY}(\lambda_\ell) P_Y(\lambda_\ell)^{-1/2} \eta_i(\lambda_\ell), \quad 1 \leq i \leq r,$$

$$f_i(\lambda_\ell) \propto P_Y(\lambda_\ell)^{-1/2} \eta_i(\lambda_\ell), \quad 1 \leq i \leq r,$$

where  $h_i(\lambda_\ell)$  and  $f_i(\lambda_\ell)$  are normalized such that  $h_i(\lambda_\ell)^H P_X(\lambda_\ell) h_i(\lambda_\ell) = 1$  and  $f_i(\lambda_\ell)^H P_Y(\lambda_\ell) f_i(\lambda_\ell) = 1$ . Here,  $\eta_i(\lambda_\ell)$  is the  $i$ th orthonormal eigenvector of  $P_Y(\lambda_\ell)^{-1/2} P_{YX}(\lambda_\ell) P_X(\lambda_\ell)^{-1} P_{XY}(\lambda_\ell) P_Y(\lambda_\ell)^{-1/2}$  corresponding to the  $i$ th largest eigenvalue  $\gamma_i(\lambda_\ell)$ . They satisfy

$$P_X(\lambda_\ell)^{-1} P_{XY}(\lambda_\ell) P_Y(\lambda_\ell)^{-1} P_{YX}(\lambda_\ell) h_i(\lambda_\ell) = \gamma_i(\lambda_\ell) h_i(\lambda_\ell),$$

$$P_Y(\lambda_\ell)^{-1} P_{YX}(\lambda_\ell) P_X(\lambda_\ell)^{-1} P_{XY}(\lambda_\ell) f_i(\lambda_\ell) = \gamma_i(\lambda_\ell) f_i(\lambda_\ell).$$

The maximum coherence between  $Z_i$  and  $W_i$  is  $\gamma_i(\lambda_\ell)$ . Moreover,  $Z_i$  and  $W_i$  have zero coherence with  $Z_j$  and  $W_j$  for  $j < i$ .

*Proof.* A proof is provided in Appendix A. □

The pair of  $Z_i$  and  $W_i$  obtained in Theorem 3.3 is called the *i*th pair of (population) canonical graph signals. Their graph coherence,  $\gamma_i(\lambda_\ell)$ , is called the *i*th (population) graph canonical coherence. The entire procedure for implementing canonical coherence analysis on graphs is referred to as ‘gCChA’.

To implement gCChA, the detailed procedure is outlined in Algorithm 1, which provides the sample versions of the canonical graph signal pairs and graph canonical coherences, denoted by  $\{(\hat{Z}_i, \hat{W}_i)\}_{i=1}^r$  and  $\hat{\gamma}_i(\lambda_\ell)$ , respectively. As shown, implementing the proposed method requires estimating the GCSDs. For this, one can use either the graph cross-periodogram or the windowed average graph cross-periodogram proposed by Kim and Oh (2025a). If multiple realizations of the two sets of graph signals  $X$  and  $Y$  are available, the graph cross-periodogram is used. If only a small number of realizations are available, the windowed average graph cross-periodogram with random windows is employed instead.

---

**Algorithm 1** gCChA

---

1: **Input:**  $S, X_1, \dots, X_p, Y_1, \dots, Y_q$   
 2: **Output:**  $\hat{Z}_1, \dots, \hat{Z}_{p \wedge q}, \hat{W}_1, \dots, \hat{W}_{p \wedge q}, \hat{\gamma}_1(\lambda_1), \dots, \hat{\gamma}_1(\lambda_n), \dots, \hat{\gamma}_{p \wedge q}(\lambda_1), \dots, \hat{\gamma}_{p \wedge q}(\lambda_n)$   
 3:  $n \leftarrow$  the number of rows in  $S$   
 4:  $r \leftarrow p \wedge q$  ▷ the number of canonical graph signals  
 5: Perform eigendecomposition:  $S = V\Lambda V^H$  ▷  $\lambda_1, \dots, \lambda_n$ : eigenvalues of  $S$

---

*Step 1 – Estimation of GCSD*

---

6: **for**  $\ell \leftarrow 1$  **to**  $n$  **do**  
 7:     Estimate spectral matrices  $P_X(\lambda_\ell), P_Y(\lambda_\ell), P_{XY}(\lambda_\ell)$ , and  $P_{YX}(\lambda_\ell)$   
 8:     and denote them by  $\hat{P}_X(\lambda_\ell), \hat{P}_Y(\lambda_\ell), \hat{P}_{XY}(\lambda_\ell)$ , and  $\hat{P}_{YX}(\lambda_\ell)$   
 9: **end for**

---

*Step 2 – Evaluation of canonical graph signals*

---

10: Estimate graph filters:  
 11: **for**  $\ell \leftarrow 1$  **to**  $n$  **do**  
 12:      $\hat{h}_i(\lambda_\ell) \leftarrow$  the  $i$ th eigenvector of  $\hat{P}_X(\lambda_\ell)^{-1}\hat{P}_{XY}(\lambda_\ell)\hat{P}_Y(\lambda_\ell)^{-1}\hat{P}_{YX}(\lambda_\ell)$   
 13:      $\hat{\gamma}_i(\lambda_\ell) \leftarrow$  the  $i$ th eigenvalue of  $\hat{P}_X(\lambda_\ell)^{-1}\hat{P}_{XY}(\lambda_\ell)\hat{P}_Y(\lambda_\ell)^{-1}\hat{P}_{YX}(\lambda_\ell)$   
 14:      $\hat{f}_i(\lambda_\ell) \leftarrow$  the  $i$ th eigenvector of  $\hat{P}_Y(\lambda_\ell)^{-1}\hat{P}_{YX}(\lambda_\ell)\hat{P}_X(\lambda_\ell)^{-1}\hat{P}_{XY}(\lambda_\ell)$   
 15: **end for**  
 16:  $\hat{H}(\lambda_\ell) := (\hat{h}_{ij}(\lambda_\ell))_{r \times p}, \quad 1 \leq \ell \leq n$   
 17:  $\hat{F}(\lambda_\ell) := (\hat{f}_{ij}(\lambda_\ell))_{r \times q}, \quad 1 \leq \ell \leq n$   
 18:  $\hat{H}_{ij} \leftarrow V \text{diag}(\{\hat{h}_{ij}(\lambda_\ell)\}_{\ell=1}^n) V^H, \quad 1 \leq i \leq r, 1 \leq j \leq p$   
 19:  $\hat{F}_{ij} \leftarrow V \text{diag}(\{\hat{f}_{ij}(\lambda_\ell)\}_{\ell=1}^n) V^H, \quad 1 \leq i \leq r, 1 \leq j \leq q$   
 20:  $\hat{Z}_i \leftarrow \hat{H}_{i1}X_1 + \dots + \hat{H}_{ip}X_p, \quad 1 \leq i \leq r$  ▷ canonical graph signal of  $X$   
 21:  $\hat{W}_i \leftarrow \hat{F}_{i1}Y_1 + \dots + \hat{F}_{iq}Y_q, \quad 1 \leq i \leq r$  ▷ canonical graph signal of  $Y$

---

### 3.2 Interpretation of Graph Canonical Coherence Analysis

We now describe how to interpret canonical graph signals. In classical CCA, interpretation is typically based on correlations between the original variables and their respective canonical variates, known as canonical loadings, rather than on the canonical coefficients themselves, which can be unstable in the presence of multicollinearity. Furthermore, correlations between the original variables and the canonical variates of the opposite set, called canonical cross-loadings, can be used to express the relationship between a variable from one set and a canonical variate from the other set. In gCChA, we similarly compute the graph coherences between the original graph signals in each dimension and the respective or opposite canonical graph signals, called *graph canonical loadings* and *graph canonical cross-loadings*, respectively. These quantities facilitate interpretation in the graph frequency domain, representing the proportion of variance in the graph Fourier coefficients of each variable that is linearly shared with the canonical graph signals from either the same set or the opposite set. Because the graph coherences contain information at each graph frequency  $\lambda_\ell$ , we can provide a multiscale interpretation across graph frequencies. For example, at a low graph frequency, a high graph coherence value between a canonical graph signal and a particular original signal indicates that they are closely related at a coarse scale. Conversely, at high graph frequency, a high graph coherence value indicates a close relationship at fine scales. An example of a more detailed interpretation is presented in Section 4.1.

Motivated by well-established terminology in classical CCA, we introduce similar quantities in the gCChA framework. The *graph canonical communality*, defined as the sum of graph canonical loadings for each canonical graph signal, indicates how much of the variance in each variable's graph Fourier coefficients can be explained by the canonical graph signals. In other words, it reflects the importance of each variable in establishing the canonical relationship between the two sets within the graph frequency domain. Specifically, the graph canonical communality of  $X_j$  at graph frequency  $\lambda_\ell$ , is given by  $\sum_{i=1}^r c_{ij}^{ZX}(\lambda_\ell)$ , and that of  $Y_j$  is  $\sum_{i=1}^r c_{ij}^{WY}(\lambda_\ell)$ , where  $c_{ij}^{ZX}(\lambda_\ell)$  and  $c_{ij}^{WY}(\lambda_\ell)$  represent the coherences between  $Z_i$  and  $X_j$  and between  $W_i$  and  $Y_j$ , respectively, at graph frequency  $\lambda_\ell$ , respectively, defined

by

$$c_{ij}^{ZX}(\lambda_\ell) = \frac{|p_{ij}^{ZX}(\lambda_\ell)|^2}{p_{ii}^Z(\lambda_\ell)p_{jj}^X(\lambda_\ell)} \quad \text{and} \quad c_{ij}^{WY}(\lambda_\ell) = \frac{|p_{ij}^{WY}(\lambda_\ell)|^2}{p_{ii}^W(\lambda_\ell)p_{jj}^Y(\lambda_\ell)}.$$

To evaluate the explanatory power of the canonical graph signals at each graph frequency  $\lambda_\ell$ , we define the *graph canonical adequacy* as the average of all graph canonical loadings for the original graph signals in a given set with respect to a single canonical graph signal. This quantity reflects how well the canonical graph signals summarize the variability of each set of graph signals at each frequency in the graph frequency domain. Specifically, the graph canonical adequacy of  $Z_i$  at graph frequency  $\lambda_\ell$  is given by  $\sum_{j=1}^p c_{ij}^{ZX}(\lambda_\ell)/p$ , and that of  $W_i$  is  $\sum_{j=1}^q c_{ij}^{WY}(\lambda_\ell)/q$ . As shown in Proposition 3.1, the graph canonical communalities range from 0 to 1, and the cumulative explanatory power, obtained by summing the graph canonical adequacies up to each component, also falls between 0 and 1. At a given graph frequency  $\lambda_\ell$ , the cumulative explanatory power of the first  $t$  ( $t \leq r$ ) canonical graph signals  $Z_1, \dots, Z_t$ , defined as  $\sum_{i=1}^t \sum_{j=1}^p c_{ij}^{ZX}(\lambda_\ell)/p$ , represents the proportion of the total variance explained by these canonical graph signals at frequency  $\lambda_\ell$  in the graph frequency domain. Similarly, the cumulative explanatory power of the first  $t$  canonical graph signals  $W_1, \dots, W_t$ , given by  $\sum_{i=1}^t \sum_{j=1}^q c_{ij}^{WY}(\lambda_\ell)/q$ , quantifies the proportion of variance explained by these canonical graph signals at frequency  $\lambda_\ell$ .

**Proposition 3.1.** *For  $1 \leq \ell \leq n$ , the following inequalities hold:*

$$\begin{aligned} 0 \leq \sum_{i=1}^r c_{ij}^{ZX}(\lambda_\ell) &\leq 1, \quad j = 1, \dots, p, \\ 0 \leq \sum_{i=1}^r c_{ij}^{WY}(\lambda_\ell) &\leq 1, \quad j = 1, \dots, q. \end{aligned}$$

Consequently,

$$0 \leq \frac{1}{p} \sum_{i=1}^r \sum_{j=1}^p c_{ij}^{ZX}(\lambda_\ell) \leq 1, \quad 0 \leq \frac{1}{q} \sum_{i=1}^r \sum_{j=1}^q c_{ij}^{WY}(\lambda_\ell) \leq 1$$

Furthermore, if  $r = \min(p, q)$ , then

$$\begin{aligned} \sum_{i=1}^r c_{ij}^{ZX}(\lambda_\ell) &= 1 \quad \text{when } p < q, \\ \sum_{i=1}^r c_{ij}^{WY}(\lambda_\ell) &= 1 \quad \text{when } p > q. \end{aligned}$$

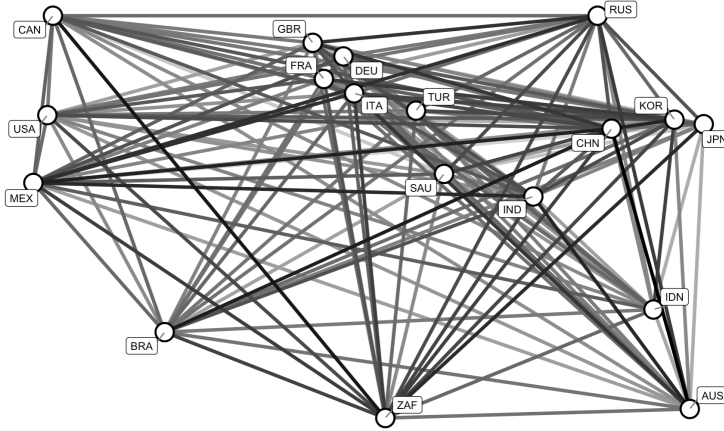


Figure 2: Trading network among G20 countries in 2019, where darker edges represent stronger trade connections.

*Proof.* A proof is provided in Appendix A. □

We note that both the interpretations and the proposition in this section directly apply to the sample versions.

## 4 Numerical Experiments

### 4.1 G20 Network Data Analysis

We apply the proposed gCChA method to data from the G20 network. From this data, we create a graph with 18 nodes, each representing a G20 country, excluding Argentina and the European Union due to missing data. The nodes are connected by edges, where each edge weight is defined as  $\log(1 + \text{trade asset})$  based on trade data from 2019 (Kim and Oh, 2025b). The resulting trading network is shown in Figure 2, and the country codes are listed in Table 1.

Two sets of observed graph signals,  $X$  and  $Y$ , represent economic and energy-related indicators, respectively. Each set consists of five graph signals, denoted as  $X = (X_1 | \dots | X_5)$  and  $Y = (Y_1 | \dots | Y_5)$ . The brief descriptions of the graph signals are provided in Table 2, with detailed definitions available in the World Bank Group's metadata glossary. All datasets were obtained from the World Bank Open Data website (<https://data.worldbank.org>).

Table 1: Country codes and their corresponding countries in the trading network

Code	Country	Code	Country	Code	Country
AUS	Australia	GBR	United Kingdom	MEX	Mexico
BRA	Brazil	IDN	Indonesia	RUS	Russian Federation
CAN	Canada	IND	India	SAU	Saudi Arabia
CHN	China	ITA	Italy	TUR	Türkiye
DEU	Germany	JPN	Japan	USA	United States of America
FRA	France	KOR	Republic of Korea	ZAF	South Africa

Table 2: List of economic and energy indicators used in the canonical graph analysis.

Signals	Indicators	Description
$X_1$	Exports of goods and services	Value of all goods and services provided to the rest of the world, including merchandise and various business services.
$X_2$	Foreign direct investment	Net inflows of investment from abroad, including equity capital, reinvestment of earnings, and other capital.
$X_3$	GDP growth	Annual percentage growth rate of GDP at market prices based on constant local currency.
$X_4$	Imports of goods and services	Value of all goods and services received from abroad, including transport and business services.
$X_5$	Inflation	Annual percentage change in the consumer price index, indicating inflation in consumer goods and services.
$Y_1$	Energy imports	Net energy imports as gross imports minus gross exports (in tons of oil equivalent).
$Y_2$	Energy use	Total primary energy consumption before transformation into other fuels.
$Y_3$	Fossil fuel consumption	Consumption of coal, oil, petroleum, and natural gas products.
$Y_4$	GDP per unit of energy use	GDP per unit of energy use, indicating energy efficiency.
$Y_5$	Renewable energy consumption	Share of renewable energy, including hydro, solar, wind, and biofuels, in total final energy consumption.

[worldbank.org/indicator](http://worldbank.org/indicator)). In summary, we have  $n = 18$ ,  $p = 5$ , and  $q = 5$ .

In implementing gCChA, we use the graph Laplacian  $L$  as GSO. The estimation of the graph power and cross-spectral densities is performed using the windowed averaging method with 50 random windows (Kim and Oh, 2025a). There are five pairs of canonical graph signals (i.e.,  $r = \min(p, q) = 5$ ),  $(\hat{Z}_1, \hat{W}_1), \dots, (\hat{Z}_5, \hat{W}_5)$ . The graph canonical coherences within each pair,  $\hat{\gamma}_1(\lambda_\ell), \dots, \hat{\gamma}_5(\lambda_\ell)$ , are shown in Figure 3, where  $\lambda_\ell$  denotes the graph frequencies of the trading network. As expected, the canonical coherences decrease from  $(\hat{Z}_1, \hat{W}_1)$  to  $(\hat{Z}_5, \hat{W}_5)$  across all graph frequencies.

From Figure 3, we observe a noticeable gap between the graph canonical coherences of  $(\hat{Z}_2, \hat{W}_2)$  and  $(\hat{Z}_3, \hat{W}_3)$ . Furthermore, we calculate the cumulative explanatory powers

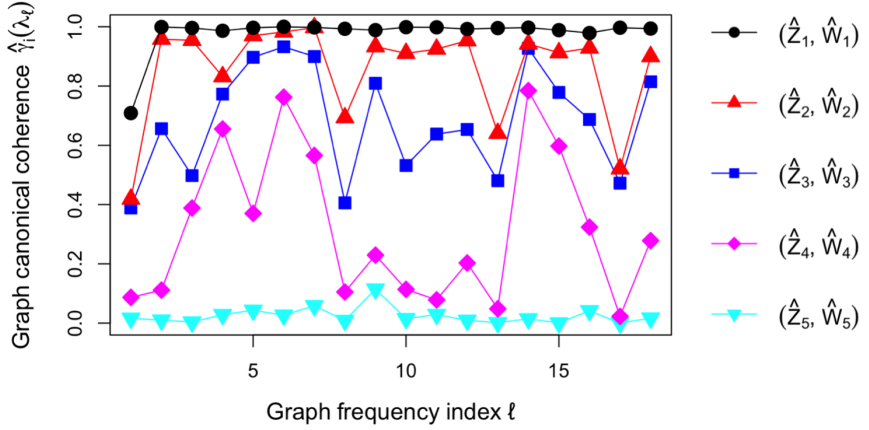


Figure 3: Graph canonical coherences  $\hat{\gamma}_i(\lambda_\ell)$  for the canonical graph signal pairs  $(\hat{Z}_i, \hat{W}_i)$ ,  $i = 1, \dots, 5$ , across graph frequencies.

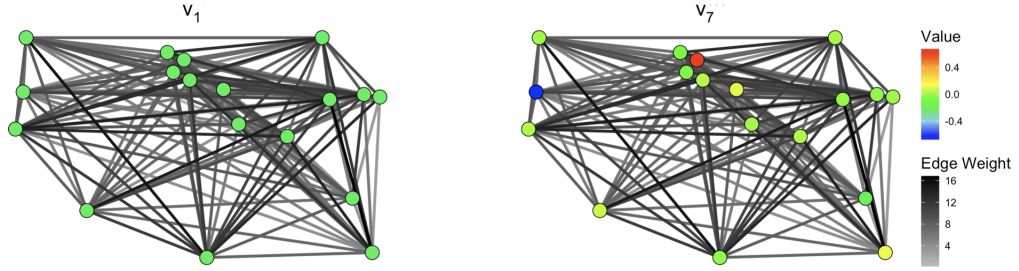


Figure 4: Basis signals  $v_1$  and  $v_7$ .

of the first two canonical graph signals,  $\sum_{i=1}^2 \sum_{j=1}^p c_{ij}^{\hat{Z}\hat{X}}(\lambda_\ell)/p$  and  $\sum_{i=1}^2 \sum_{j=1}^q c_{ij}^{\hat{W}\hat{Y}}(\lambda_\ell)/q$ , which exceed 0.75, indicating that more than 75% of the variance within  $X$  and  $Y$ , on average across graph frequencies, is explained by the first two respective canonical graph signals. So, we interpret the first two canonical pairs in detail. Although interpretation can be applied at each graph frequency, we examine  $\lambda_1$  and  $\lambda_7$  as representative frequencies for coarse and fine scales, respectively. Figure 4 shows the associated basis signals, labeled  $v_1$  and  $v_7$ . The basis signal  $v_1$  is constant across all nodes, representing the overall pattern among the G20 countries at the coarsest scale. In contrast,  $v_7$ , corresponding to a finer scale, highlights the contrast between Germany and the United States.

At the lowest graph frequency  $\lambda_1$ , the canonical graph signals depict broad, overall rela-

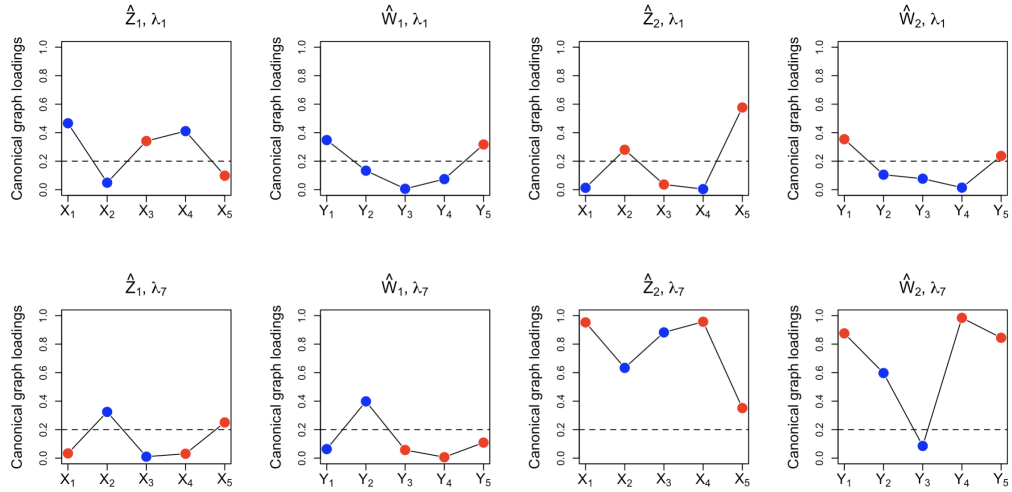


Figure 5: Graph canonical loadings of the first two canonical graph signals at graph frequencies  $\lambda_1$  (top row) and  $\lambda_7$  (bottom row). Red dots show positive correlations in the frequency domain, while blue dots represent negative correlations. Loadings with a magnitude exceeding 0.2 (shown by the dashed line) are used for interpretation.

tionships across the G20 network, capturing country-level similarity patterns that dominate at a global scale, as reflected by the constant basis signal  $v_1$ . At this frequency, as shown in the top row of Figure 5,  $\hat{Z}_1$  is associated with  $X_1$ ,  $X_3$ , and  $X_4$  in the  $(-), (+), (-)$  directions, while  $\hat{W}_1$  is associated with  $Y_1$  and  $Y_5$  in the  $(-)$  and  $(+)$  directions, respectively. Therefore, the first canonical pair  $(\hat{Z}_1, \hat{W}_1)$  shows that countries with higher GDP growth but lower trade volumes tend to have lower energy import dependence and higher use of renewable energy. Countries such as France, the United Kingdom, Canada, Australia, and Brazil exhibit this pattern, reflecting growth- and sustainability-focused systems characterized by moderate trade activity, steady growth, and a relatively high level of energy independence supported by renewables, which tends to increase both  $\hat{Z}_1$  and  $\hat{W}_1$ . In contrast, export- and industry-driven countries like Korea, Japan, Italy, India, and Türkiye show the opposite trend, causing both  $\hat{Z}_1$  and  $\hat{W}_1$  to decrease. This reflects their stronger trade dependence and higher reliance on energy imports, along with lower adoption of renewables. This canonical relationship effectively captures a broad, global-scale trade-energy connection across the G20 network, as the correlation between  $\hat{Z}_1$  and  $\hat{W}_1$  at graph

frequency  $\lambda_1$  reflects a consistent structural pattern shared by many countries.

For the second canonical pair,  $\hat{Z}_2$  is associated with  $X_2$  and  $X_5$ , and  $\hat{W}_2$  with  $Y_1$  and  $Y_5$ , all in the (+) direction. This pair indicates that countries with higher levels of foreign direct investment (FDI) and inflation tend to have greater energy imports and increased use of renewable energy. This reflects a pattern that economies with greater openness and inflation pressures simultaneously increase energy imports and pursue energy transition policies. Countries such as China and India, known for rapid industrial growth, substantial FDI inflows, and ongoing renewable investments, tend to push both  $\hat{Z}_2$  and  $\hat{W}_2$  higher. In contrast, Canada, Australia, and Saudi Arabia, which are resource-based and domestically stable economies with low inflation and limited reliance on imported energy, tend to pull these variables lower. Overall, the coarse-scale canonical signals show the main relationships between economic openness, price trends, and energy transition observed across the G20 network.

At the high graph frequency  $\lambda_7$ , the canonical graph signals highlight fine-scale, country-specific contrasts within the G20 trade–energy network, particularly between Germany and the United States, as illustrated by the corresponding basis signal  $v_7$ . For the first canonical pair,  $\hat{Z}_1$  is associated with  $X_2$  and  $X_5$  in the (–) and (+) directions, while  $\hat{W}_1$  is associated with  $Y_2$  in the (–) direction. This relationship indicates that countries with lower FDI inflows and less total energy consumption tend to have higher values of  $(\hat{Z}_1, \hat{W}_1)$ . Germany, known for relatively modest FDI inflows but efficient and moderate energy use, tends to have higher values of  $\hat{Z}_1$  and  $\hat{W}_1$ . In contrast, the United States, which has higher FDI inflows and greater energy consumption, tends to be associated with smaller values of  $\hat{Z}_1$  and  $\hat{W}_1$ .

The second canonical pair exhibits a more complex structure:  $\hat{Z}_2$  is associated with  $X_1, X_2, X_3, X_4$ , and  $X_5$  in the (+), (–), (–), (+), (+) directions, while  $\hat{W}_2$  is connected to  $Y_1, Y_2, Y_4$ , and  $Y_5$  in the (+), (–), (+), (+) directions, respectively. Unlike the first pair, which mainly shows the connection between capital inflows and energy use, this pair illustrates interconnected relationships among trade dependence, economic growth, and renewable energy strategies. Germany, known for its high trade openness, moderate GDP growth, reliance on imported energy, and strong energy efficiency, tends to have

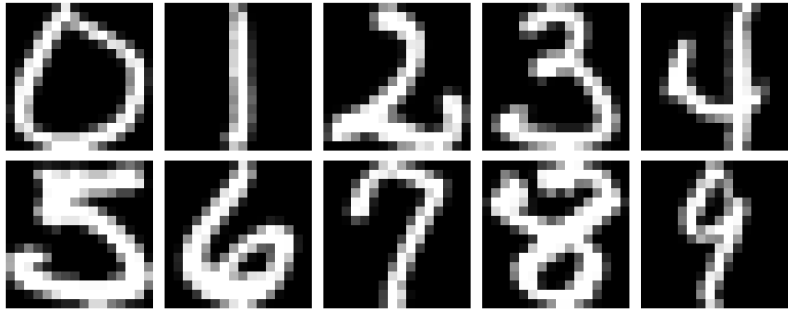


Figure 6: Illustration of the USPS dataset.

larger values of  $\hat{Z}_2$  and  $\hat{W}_2$ . In contrast, the United States, which is often described as having lower trade dependence, higher GDP growth, and less reliance on energy imports, tends to have smaller values of  $\hat{Z}_2$  and  $\hat{W}_2$ . Overall, the high-frequency canonical signals at  $\lambda_7$  emphasize localized variations that distinguish advanced economies with differing structural balances among industrial openness, energy efficiency, and policy direction.

## 4.2 Classification Analysis of USPS Dataset

We compare the proposed gCChA with the gCCA method of Chen et al. (2018) through an image classification task. For this purpose, we consider the USPS dataset, which consists of handwritten digit images obtained by automatically scanning envelopes from the United States Postal Service (Hull, 1994). The dataset contains  $16 \times 16$  grayscale images of digits from 0 to 9, as illustrated in Figure 6.

We use a total of 400 images, with 40 images per digit class. Following the classification method in Chen et al. (2018), we construct a graph where each image is a node. We connect nodes that share the same digit label and assign edge weights based on cosine similarities computed from the original 256-dimensional pixel vectors. Then, we split the 256 ( $= 16 \times 16$ ) pixel features of each image into two parts. Specifically, the first part corresponds to the top  $K$  rows (out of 16 total rows), forming a  $(16 \times K)$ -dimensional graph signal, while the second part corresponds to the remaining  $(16 - K)$  rows, forming a  $(16 \times (16 - K))$ -dimensional graph signal. We consider five partitions with  $K \in \{4, 6, 8, 10, 12\}$ . For each image, these two parts define two graph signals.

Table 3: USPS dataset classification results. Each cell shows the average classification accuracy across 50 repetitions, with standard deviations in parentheses.

$r$	Methods	$K/16$				
		0.25	0.375	0.5	0.625	0.75
20	gCCA	0.979 (0.007)	0.971 (0.007)	0.967 (0.009)	0.972 (0.008)	0.980 (0.006)
	gCChA	0.992 (0.006)	0.993 (0.005)	0.993 (0.006)	0.991 (0.007)	0.993 (0.004)
40	gCCA	0.948 (0.009)	0.923 (0.012)	0.904 (0.017)	0.913 (0.011)	0.932 (0.011)
	gCChA	0.999 (0.001)	0.999 (0.001)	0.999 (0.000)	0.999 (0.001)	0.999 (0.001)

For each partition, we compute  $r$  pairs of canonical graph signals, where  $r \in \{20, 40\}$ . We concatenate the two  $r$ -dimensional signals to form a  $2r$ -dimensional feature vector as the new representation for each image. Then, we classify using a 10-nearest-neighbor classifier in this transformed space. We run the classification experiment 50 times. In each run, we randomly select 400 images (40 per digit class) from the dataset, construct the graph, compute the canonical graph signals, and assess classification accuracy. The comparison is based on the average accuracy over 50 repetitions.

Hyperparameter tuning for gCCA follows the procedure in Chen et al. (2018), where tuning is performed over logarithmically spaced values between  $10^{-3}$  and  $10^3$ . We note an important conceptual difference between the two approaches: Chen et al. (2018) evaluated test accuracies by projecting test images onto the learned canonical vectors from the training set, whereas in gCChA, the graph filtering operations rely on the topology of the underlying graph. Because the graph constructed from test images generally differs from that constructed from training images, the filters learned from training cannot be directly applied to test images. In particular, when the number of images in the training and test sets differs, the corresponding matrix dimensions do not match, and filtering operations cannot be performed. As a result, the comparison between gCCA and gCChA is based on training accuracy.

Table 3 summarizes the classification performance. Across all proportions of the first part ( $= K/16$ ), the proposed gCChA consistently achieves higher accuracy. These results suggest that gCChA can be effectively applied in image classification tasks.

## 5 Concluding Remarks

In this paper, we propose a graph canonical coherence analysis (gCChA) method that operates in the graph frequency domain. The proposed method handles two multivariate graph signals defined on the same graph and produces two canonical graph signals that serve as low-dimensional representations summarizing the dependence structure between the two and capturing their shared information. The proposed framework offers a spectral interpretation of canonical graph signals by associating them with the original graph signals at each graph frequency. We demonstrated its applicability through analyses of real-world datasets, including the G20 network economic-energy dataset and the USPS handwritten image dataset. The results showed that the canonical graph signals allow meaningful spectral interpretation and achieve superior classification performance compared with existing methods operating in the node domain.

There are several promising directions for future research. One avenue is to extend the current framework to accommodate more than two graph datasets, enabling canonical dependence analysis among multiple graph signals. Another direction is to explore different application areas where multiple graph-structured datasets coexist, such as brain functional networks and environmental sensing networks. Further methodological development remains of interest. Specifically, enhanced estimation strategies for GCSDs could be explored, including research into the optimal window design for the windowed average graph cross-periodogram. We leave these topics for future investigation.

## Acknowledgments

This research was supported by the National Research Foundation of Korea (NRF) funded by the Korea government (2021R1A2C1091357) and by Basic Science Research Program through the NRF grant funded by the Ministry of Education (RS-2021-NR060140).

## Data Availability Statement

The economic and energy datasets for G20 countries, as well as the USPS handwritten digit dataset, are available on GitHub at <https://github.com/qsoon/gCChA>.

## Appendix A Proofs

### A.1 Proof of Theorem 3.1

*Proof.* Denote the error to be minimized by  $J$ . Then, using (2), the error becomes

$$\begin{aligned}
J &= \sum_{i=1}^q E[(Y_i - (\mu_i + \mathcal{T}_i^G(Z)))^H (Y_i - (\mu_i + \mathcal{T}_i^G(Z)))] \\
&= \sum_{i=1}^q \text{tr}[E[(Y_i - (\mu_i + \mathcal{T}_i^G(Z)))(Y_i - (\mu_i + \mathcal{T}_i^G(Z))^H]] \\
&= \sum_{i=1}^q \text{tr}[E[\{(Y_i - \mu_i^Y - \sum_{j=1}^r G_{ij}(Z_j - \mu_j^Z)) + (\mu_i^Y - \mu_i - \sum_{j=1}^r G_{ij}\mu_j^Z)\} \\
&\quad \{(Y_i - \mu_i^Y - \sum_{j=1}^r G_{ij}(Z_j - \mu_j^Z)) + (\mu_i^Y - \mu_i - \sum_{j=1}^r G_{ij}\mu_j^Z)\}^H]], 
\end{aligned}$$

where  $Z_j$  is defined by (1), and  $\mu_j^Z = E[Z_j] = \sum_{k=1}^p H_{jk}\mu_k^X$ . Note that  $\sum_{j=1}^r G_{ij}(Z_j - \mu_j^Z) = \sum_{j=1}^r G_{ij}(\sum_{k=1}^p H_{jk}(X_k - \mu_k^X)) = \sum_{j=1}^p A_{ij}(X_j - \mu_j^X)$ . Consequently,

$$\begin{aligned}
J &= \sum_{i=1}^q \text{tr}[E[\{(Y_i - \mu_i^Y - \sum_{j=1}^p A_{ij}(X_j - \mu_j^X)) + (\mu_i^Y - \mu_i - \sum_{j=1}^r G_{ij}\mu_j^Z)\} \\
&\quad \{(Y_i - \mu_i^Y - \sum_{j=1}^p A_{ij}(X_j - \mu_j^X)) + (\mu_i^Y - \mu_i - \sum_{j=1}^r G_{ij}\mu_j^Z)\}^H]] \\
&= \sum_{i=1}^q \text{tr}[\Sigma_{ii}^Y - \sum_{j=1}^p A_{ij}\Sigma_{ji}^{XY} - \sum_{j=1}^p \Sigma_{ij}^{YX}A_{ij}^H + \sum_{1 \leq j, k \leq p} A_{ij}\Sigma_{jk}^X A_{ik}^H \\
&\quad + \sum_{i=1}^q (\mu_i^Y - \mu_i - \sum_{j=1}^r G_{ij}\mu_j^Z)^H(\mu_i^Y - \mu_i - \sum_{j=1}^r G_{ij}\mu_j^Z) \\
&= \sum_{\ell=1}^n \underbrace{\left[ \sum_{i=1}^q \left\{ p_{ii}^Y(\lambda_\ell) - \sum_{j=1}^p a_{ij}(\lambda_\ell)p_{ji}^{XY}(\lambda_\ell) - \sum_{j=1}^p p_{ij}^{YX}(\lambda_\ell)a_{ij}^*(\lambda_\ell) + \sum_{1 \leq j, k \leq p} a_{ij}(\lambda_\ell)p_{jk}^X(\lambda_\ell)a_{ik}^*(\lambda_\ell) \right\} \right]}_{J(\lambda_\ell)} \\
&\quad + \sum_{i=1}^q (\mu_i^Y - \mu_i - \sum_{j=1}^r G_{ij}\mu_j^Z)^H(\mu_i^Y - \mu_i - \sum_{j=1}^r G_{ij}\mu_j^Z), \tag{A.1}
\end{aligned}$$

where  $A_{ij} = V \text{diag}(\{a_{ij}(\lambda_\ell)\}_{\ell=1}^n) V^H$ , and  $\Sigma_{ij}^X$ ,  $\Sigma_{ij}^Y$ ,  $\Sigma_{ij}^{XY}$ , and  $\Sigma_{ij}^{YX}$  are the cross-covariance matrices between  $X_i$  and  $X_j$ ,  $Y_i$  and  $Y_j$ ,  $X_i$  and  $Y_j$ , and  $Y_i$  and  $X_j$ , respectively. If we compute the solutions  $H_{ij}$  and  $G_{ij}$  that minimize  $J$ , we obtain the solution

$$\mu_i = \mu_i^Y - \sum_{j=1}^r G_{ij}\mu_j^Z = \mu_i^Y - \sum_{j=1}^r G_{ij} \left( \sum_{k=1}^p H_{jk}\mu_k^X \right),$$

which makes the latter term on the right-hand side of (A.1) equal to zero.

Now, let us find the solutions minimizing the former term on the right-hand side of (A.1). To achieve this, we need to minimize  $J(\lambda)$  for each  $\lambda_\ell$  ( $1 \leq \ell \leq n$ ). Define the matrices  $A(\lambda_\ell)$ ,  $H(\lambda_\ell)$ , and  $G(\lambda_\ell)$  as  $q \times p$ ,  $r \times p$ , and  $q \times r$  matrices, respectively, where the  $(i, j)$ th elements are  $a_{ij}(\lambda_\ell)$ ,  $h_{ij}(\lambda_\ell)$ , and  $g_{ij}(\lambda_\ell)$ , representing the frequency responses of the graph filters  $A_{ij}$ ,  $H_{ij}$ , and  $G_{ij}$ , respectively. Then, we have  $A(\lambda_\ell) = G(\lambda_\ell)H(\lambda_\ell)$ , implying that  $\text{rank}(A(\lambda_\ell)) \leq r$ . Moreover, Corollary 3.1 in Kim and Oh (2024) ensures

that  $P_X^{1/2}(\lambda_\ell)$  exists. With this in mind,  $J(\lambda_\ell)$  becomes

$$\begin{aligned} J(\lambda_\ell) &= \text{tr}[P_Y(\lambda_\ell) - A(\lambda_\ell)P_{XY}(\lambda_\ell) - P_{YX}(\lambda_\ell)A(\lambda_\ell)^H + A(\lambda_\ell)P_X(\lambda_\ell)A(\lambda_\ell)^H] \\ &= \text{tr}[P_Y(\lambda_\ell) - P_{YX}(\lambda_\ell)P_X(\lambda_\ell)^{-1}P_{XY}(\lambda_\ell)] \\ &\quad + \text{tr}[(P_{YX}(\lambda_\ell)P_X(\lambda_\ell)^{-1/2} - A(\lambda_\ell)P_X(\lambda_\ell)^{1/2})(P_{YX}(\lambda_\ell)P_X(\lambda_\ell)^{-1/2} - A(\lambda_\ell)P_X(\lambda_\ell)^{1/2})^H]. \end{aligned}$$

The  $i$ th eigenvectors of  $P_{YX}(\lambda_\ell)P_X(\lambda_\ell)^{-1}P_{XY}(\lambda_\ell)$  and  $P_X(\lambda_\ell)^{-1/2}P_{XY}(\lambda_\ell)P_{YX}(\lambda_\ell)P_X(\lambda_\ell)^{-1/2}$  are denoted by  $u_i(\lambda_\ell)$  and  $v_i(\lambda_\ell)$ , respectively. Nonzero eigenvalues of the two matrices are equal by Theorem 3.7.2 of Brillinger (2001) and we denote the  $i$ th eigenvalue of  $P_{YX}(\lambda_\ell)P_X(\lambda_\ell)^{-1}P_{XY}(\lambda_\ell)$  by  $\tau_i(\lambda_\ell)$ . Thus, by Corollary 3.7.4 of Brillinger (2001),  $J(\lambda_\ell)$  is minimized when

$$A(\lambda_\ell)P_X(\lambda_\ell)^{1/2} = \sum_{i=1}^r \tau_i(\lambda_\ell)^{1/2} u_i(\lambda_\ell) v_i(\lambda_\ell)^H.$$

Therefore, the indicated  $A(\lambda_\ell) = G(\lambda_\ell)H(\lambda_\ell)$  minimizes  $J(\lambda_\ell)$ .

For the minimizing solution discussed above, we have  $P_{YX}(\lambda_\ell)P_X(\lambda_\ell)^{-1/2} - A(\lambda_\ell)P_X(\lambda_\ell)^{1/2} = \sum_{i>r} \tau_i(\lambda_\ell)^{1/2} u_i(\lambda_\ell) v_i(\lambda_\ell)^H$ . Therefore,  $J(\lambda_\ell)$  becomes  $\text{tr}[P_Y(\lambda_\ell) - P_{YX}(\lambda_\ell)P_X(\lambda_\ell)^{-1}P_{XY}(\lambda_\ell)] + \sum_{i>r} \tau_i(\lambda_\ell)$ . Consequently, the minimum mean squared error is obtained as  $\sum_{\ell=1}^n \text{tr}[P_Y(\lambda_\ell) - P_{YX}(\lambda_\ell)P_X(\lambda_\ell)^{-1}P_{XY}(\lambda_\ell)] + \sum_{\ell=1}^n \sum_{i>r} \tau_i(\lambda_\ell)$ . This completes the proof.  $\square$

## A.2 Proof of Theorem 3.2

*Proof.* Denote the error to be minimized by  $J_0$ . Then, the error becomes

$$\begin{aligned} J_0 &= \sum_{i=1}^r E[(W_i - \mu_i - Z_i)^H (W_i - \mu_i - Z_i)] = \sum_{i=1}^r \text{tr}[E[(W_i - \mu_i - Z_i)(W_i - \mu_i - Z_i)^H]] \\ &= \sum_{i=1}^r \text{tr}[E[\{(W_i - \mu_i^W - (Z_i - \mu_i^Z)) + (\mu_i^W - \mu_i - \mu_i^Z)\} \\ &\quad \{(W_i - \mu_i^W - (Z_i - \mu_i^Z)) + (\mu_i^W - \mu_i - \mu_i^Z)\}^H]], \end{aligned}$$

where  $\mu_i^Z = E[Z_i] = \sum_{j=1}^p H_{ij}\mu_j^X$  and  $\mu_i^W = E[W_i] = \sum_{j=1}^p F_{ij}\mu_j^Y$ . Similar to the proof of Theorem 3.1,

$$\begin{aligned}
J_0 &= \sum_{i=1}^r \text{tr} \left[ \sum_{1 \leq j, k \leq q} F_{ij}\Sigma_{jk}^Y F_{ik}^H - \sum_{1 \leq j \leq p, 1 \leq k \leq q} H_{ij}\Sigma_{jk}^{XY} F_{ik}^H - \sum_{1 \leq j \leq p, 1 \leq k \leq q} F_{ik}\Sigma_{kj}^{YX} H_{ij}^H + \sum_{1 \leq j, k \leq p} H_{ij}\Sigma_{jk}^X H_{ik}^H \right] \\
&\quad + \sum_{i=1}^r \left( \sum_{j=1}^q F_{ij}\mu_j^Y - \mu_i - \sum_{j=1}^p H_{ij}\mu_j^X \right)^H \left( \sum_{j=1}^q F_{ij}\mu_j^Y - \mu_i - \sum_{j=1}^p H_{ij}\mu_j^X \right) \\
&= \sum_{\ell=1}^n \left[ \sum_{i=1}^r \left\{ \sum_{1 \leq j, k \leq q} f_{ij}(\lambda_\ell) p_{jk}^Y(\lambda_\ell) f_{ik}^*(\lambda_\ell) - \sum_{1 \leq j \leq p, 1 \leq k \leq q} h_{ij}(\lambda_\ell) p_{jk}^{XY}(\lambda_\ell) f_{ik}^*(\lambda_\ell) \right. \right. \\
&\quad \left. \left. - \sum_{1 \leq j \leq p, 1 \leq k \leq q} f_{ik}(\lambda_\ell) p_{ij}^{YX}(\lambda_\ell) h_{ij}^*(\lambda_\ell) + \sum_{1 \leq j, k \leq p} h_{ij}(\lambda_\ell) p_{jk}^X(\lambda_\ell) h_{ik}^*(\lambda_\ell) \right\} \right] \\
&\quad + \sum_{i=1}^r \left( \sum_{j=1}^q F_{ij}\mu_j^Y - \mu_i - \sum_{j=1}^p H_{ij}\mu_j^X \right)^H \left( \sum_{j=1}^q F_{ij}\mu_j^Y - \mu_i - \sum_{j=1}^p H_{ij}\mu_j^X \right) \\
&=: \sum_{\ell=1}^n J_0(\lambda_\ell) + \sum_{i=1}^r \left( \sum_{j=1}^q F_{ij}\mu_j^Y - \mu_i - \sum_{j=1}^p H_{ij}\mu_j^X \right)^H \left( \sum_{j=1}^q F_{ij}\mu_j^Y - \mu_i - \sum_{j=1}^p H_{ij}\mu_j^X \right). \tag{A.2}
\end{aligned}$$

If we compute the solutions  $H_{ij}$  and  $F_{ij}$  that minimize  $J_0$ , we obtain the solution

$$\mu_i = \sum_{j=1}^q F_{ij}\mu_j^Y - \sum_{j=1}^p H_{ij}\mu_j^X,$$

which makes the latter term on the right-hand side of (A.2) equal to zero.

The expression  $J_0(\lambda_\ell)$  can be reformulated as

$$\begin{aligned}
J_0(\lambda_\ell) &= \text{tr}[F(\lambda_\ell)P_Y(\lambda_\ell)F(\lambda_\ell)^H - H(\lambda_\ell)P_{XY}(\lambda_\ell)F(\lambda_\ell)^H \\
&\quad - F(\lambda_\ell)P_{YX}(\lambda_\ell)H(\lambda_\ell)^H + H(\lambda_\ell)P_X(\lambda_\ell)H(\lambda_\ell)^H].
\end{aligned}$$

The proof is then completed by following a similar procedure to that in Theorem 10.2.2 of Brüllinger (2001).  $\square$

### A.3 Proof of Theorem 3.3

*Proof.* We have  $\Sigma_{ii}^Z = \mathbb{E}[(\sum_{j=1}^p H_{ij}X_j)(\sum_{k=1}^p H_{ik}X_k)^H] = \sum_{1 \leq j, k \leq p} H_{ij}\Sigma_{jk}^X H_{ik}^H$ . Then, we can easily derive  $p_{ii}^Z(\lambda_\ell) = h_i(\lambda_\ell)^H P_X(\lambda_\ell)h_i(\lambda_\ell)$ . Similarly, we can get  $p_{ii}^W(\lambda_\ell) =$

$g_i(\lambda_\ell)^H P_Y(\lambda_\ell) g_i(\lambda_\ell)$  and  $p_{ii}^{ZW}(\lambda_\ell) = h_i(\lambda_\ell)^H P_{XY}(\lambda_\ell) g_i(\lambda_\ell)$ . Therefore, the coherence of  $Z_i$  and  $W_i$  at  $\lambda_\ell$ , defined by  $c_{ii}^{ZW}(\lambda_\ell) = |p_{ii}^{ZW}(\lambda_\ell)|^2 / (p_{ii}^Z(\lambda_\ell) p_{ii}^W(\lambda_\ell))$ , satisfies the following inequalities for  $h'_i(\lambda_\ell) = P_X(\lambda_\ell)^{1/2} h_i(\lambda_\ell)$  and  $f'_i(\lambda_\ell) = P_Y(\lambda_\ell)^{1/2} f_i(\lambda_\ell)$ .

$$\begin{aligned} c_{ii}^{ZW}(\lambda_\ell) &= \frac{|h'_i(\lambda_\ell)^H P_X(\lambda_\ell)^{-1/2} P_{XY}(\lambda_\ell) P_Y(\lambda_\ell)^{-1/2} f'_i(\lambda_\ell)|^2}{(h'_i(\lambda_\ell)^H h'_i(\lambda_\ell))(f'_i(\lambda_\ell)^H f'_i(\lambda_\ell))} \\ &\leq \frac{f'_i(\lambda_\ell)^H (P_Y(\lambda_\ell)^{-1/2} P_{YX}(\lambda_\ell) P_X(\lambda_\ell)^{-1} P_{XY}(\lambda_\ell) P_Y(\lambda_\ell)^{-1/2}) f'_i(\lambda_\ell)}{f'_i(\lambda_\ell)^H f'_i(\lambda_\ell)} \\ &\leq \gamma_i(\lambda_\ell). \end{aligned}$$

The first inequality holds by Cauchy–Schwarz inequality. The second inequality follows from the maximization property of quadratic forms. The equation in the second inequality is obtained when  $f'_i(\lambda_\ell)$  is proportional to  $\eta_i(\lambda_\ell)$ . The equation in the first inequality is obtained when  $h'_i(\lambda_\ell)$  is proportional to  $P_X(\lambda_\ell)^{-1/2} P_{XY}(\lambda_\ell) P_Y(\lambda_\ell)^{-1/2} \eta_i(\lambda_\ell)$ . Therefore, the solutions  $h_i(\lambda_\ell)$  and  $f_i(\lambda_\ell)$  are proportional to  $P_X(\lambda_\ell)^{-1} P_{XY}(\lambda_\ell) P_Y(\lambda_\ell)^{-1/2} \eta_i(\lambda_\ell)$  and  $P_Y(\lambda_\ell)^{-1/2} \eta_i(\lambda_\ell)$ , respectively. From the above inequality, the maximum coherence is given by  $\gamma_i(\lambda_\ell)$ .

We note that for the solutions  $h_i(\lambda_\ell)$  and  $f_i(\lambda_\ell)$ , the associated quantity  $h'_i(\lambda_\ell)$  is the normalized eigenvector of

$$P_X(\lambda_\ell)^{-1/2} P_{XY}(\lambda_\ell) P_Y(\lambda_\ell)^{-1} P_{YX}(\lambda_\ell) P_X(\lambda_\ell)^{-1/2}$$

corresponding to the eigenvalue  $\gamma_i(\lambda_\ell)$ , and that  $f'_i(\lambda_\ell)$  is the normalized  $\eta_i(\lambda_\ell)$ . It is clear that

$$\begin{aligned} P_X(\lambda_\ell)^{-1} P_{XY}(\lambda_\ell) P_Y(\lambda_\ell)^{-1} P_{YX}(\lambda_\ell) h_i(\lambda_\ell) &= \gamma_i(\lambda_\ell) h_i(\lambda_\ell), \\ P_Y(\lambda_\ell)^{-1} P_{YX}(\lambda_\ell) P_X(\lambda_\ell)^{-1} P_{XY}(\lambda_\ell) f_i(\lambda_\ell) &= \gamma_i(\lambda_\ell) f_i(\lambda_\ell). \end{aligned}$$

In addition, for these solutions, we have  $p_{ii}^Z(\lambda_\ell) = h_i(\lambda_\ell)^H P_X(\lambda_\ell) h_i(\lambda_\ell) = 1$  and  $p_{ii}^W(\lambda_\ell) = f_i(\lambda_\ell)^H P_Y(\lambda_\ell) f_i(\lambda_\ell) = 1$ . Moreover,  $p_{ij}^Z(\lambda_\ell) = h_i(\lambda_\ell)^H P_X(\lambda_\ell) h_j(\lambda_\ell) = h'_i(\lambda_\ell)^H h'_j(\lambda_\ell)$ , which is equal to zero for  $j < i$ . Similarly,  $p_{ij}^W(\lambda_\ell) = 0$  for  $j < i$ . It also holds that  $p_{ij}^{ZW}(\lambda_\ell) = h_i(\lambda_\ell)^H P_{XY}(\lambda_\ell) f_j(\lambda_\ell) = h'_i(\lambda_\ell)^H P_X(\lambda_\ell)^{-1/2} P_{XY}(\lambda_\ell) P_Y(\lambda_\ell)^{-1/2} f'_j(\lambda_\ell)$  is proportional to  $\eta_i(\lambda_\ell)^H P_Y(\lambda_\ell)^{-1/2} P_{YX}(\lambda_\ell) P_X(\lambda_\ell)^{-1} P_{XY}(\lambda_\ell) P_Y(\lambda_\ell)^{-1/2} \eta_j(\lambda_\ell) = 0$  for  $j < i$ . Similarly,  $p_{ij}^{WZ}(\lambda_\ell) = 0$  for  $j < i$ . Therefore, the graph coherences between  $Z_i$  and  $Z_j$ ,  $W_j$  for  $j < i$  are zeros and those between  $W_i$  and  $Z_j$ ,  $W_j$  for  $j < i$  are zeros.  $\square$

## A.4 Proof of Proposition 3.1

*Proof.* The coherence of  $Z_i$  and  $X_j$  at graph frequency  $\lambda_\ell$  is defined as

$$c_{ij}^{ZX}(\lambda_\ell) = \frac{|p_{ij}^{ZX}(\lambda_\ell)|^2}{p_{ii}^Z(\lambda_\ell)p_{jj}^X(\lambda_\ell)}.$$

For the canonical basis vector  $e_j = (0, \dots, 0, 1, 0, \dots, 0)^\top$ , this becomes

$$c_{ij}^{ZX}(\lambda_\ell) = \frac{|h_i(\lambda_\ell)^H P_X(\lambda_\ell) e_j|^2}{e_j^H P_X(\lambda_\ell) e_j} = \frac{e_j^H P_X(\lambda_\ell) h_i(\lambda_\ell) h_i(\lambda_\ell)^H P_X(\lambda_\ell) e_j}{e_j^H P_X(\lambda_\ell) e_j}.$$

Then,

$$\sum_{i=1}^r c_{ij}^{ZX}(\lambda_\ell) = \frac{e_j^H P_X(\lambda_\ell) H(\lambda_\ell)^H H(\lambda_\ell) P_X(\lambda_\ell) e_j}{e_j^H P_X(\lambda_\ell) e_j}.$$

By the maximization property of quadratic forms, the maximum value of  $\sum_{i=1}^r c_{ij}^{ZX}(\lambda_\ell)$  corresponds to the largest eigenvalue of  $P_X(\lambda_\ell)^{1/2} H(\lambda_\ell)^H H(\lambda_\ell) P_X(\lambda_\ell)^{1/2}$ . Since  $H(\lambda_\ell) P_X(\lambda_\ell) H(\lambda_\ell)^H = I_r$ , the matrix  $P_X(\lambda_\ell)^{1/2} H(\lambda_\ell)^H H(\lambda_\ell) P_X(\lambda_\ell)^{1/2}$  is Hermitian and idempotent. Therefore, its eigenvalues are either 0 or 1, and hence,

$$\sum_{i=1}^r c_{ij}^{ZX}(\lambda_\ell) \leq 1.$$

Similarly,

$$\sum_{i=1}^r c_{ij}^{WY}(\lambda_\ell) \leq 1.$$

Consequently,

$$\frac{1}{p} \sum_{i=1}^r \sum_{j=1}^p c_{ij}^{ZX}(\lambda_\ell) \leq 1, \quad \frac{1}{q} \sum_{i=1}^r \sum_{j=1}^q c_{ij}^{WY}(\lambda_\ell) \leq 1.$$

The non-negativity is obvious.

In the special case where  $r = \min(p, q)$ , consider first the case  $p > q$  ( $r = q$ ). From  $F(\lambda_\ell) P_Y(\lambda_\ell) F(\lambda_\ell)^H = I_q$ , it follows that  $P_Y(\lambda_\ell)^{1/2} F(\lambda_\ell)^H F(\lambda_\ell) P_Y(\lambda_\ell)^{1/2} = I_q$ . Thus,  $\sum_{i=1}^r c_{ij}^{WY}(\lambda_\ell) = 1$ . Similarly, if  $p < q$  ( $r = p$ ), then  $\sum_{i=1}^r c_{ij}^{ZX}(\lambda_\ell) = 1$ .  $\square$

## References

Andrew, G., Arora, R., Bilmes, J., and Livescu, K. (2013). Deep canonical correlation analysis. In *Proceedings of the 30th International Conference on Machine Learning*, volume 28, pages 1247–1255.

Bach, F. R. and Jordan, M. I. (2005). A probabilistic interpretation of canonical correlation analysis. Technical Report 688, Department of Statistics, University of California, Berkeley.

Brillinger, D. R. (2001). *Time Series: Data Analysis and Theory*. SIAM.

Chen, J., Wang, G., and Giannakis, G. B. (2019). Graph multiview canonical correlation analysis. *IEEE Transactions on Signal Processing*, 67(11):2826–2838.

Chen, J., Wang, G., Shen, Y., and Giannakis, G. B. (2018). Canonical correlation analysis of datasets with a common source graph. *IEEE Transactions on Signal Processing*, 66(16):4398–4408.

Cichonska, A., Rousu, J., Marttinen, P., Kangas, A. J., Soininen, P., Lehtimäki, T., Raitakari, O. T., Järvelin, M.-R., Salomaa, V., Ala-Korpela, M., et al. (2016). metaCCA: Summary statistics-based multivariate meta-analysis of genome-wide association studies using canonical correlation analysis. *Bioinformatics*, 32(13):1981–1989.

Girault, B. (2015). Stationary graph signals using an isometric graph translation. In *2015 23rd European Signal Processing Conference (EUSIPCO)*, pages 1516–1520. IEEE.

Hardoon, D. R., Szedmak, S., and Shawe-Taylor, J. (2004). Canonical correlation analysis: An overview with application to learning methods. *Neural Computation*, 16(12):2639–2664.

Hotelling, H. (1935). The most predictable criterion. *Journal of Educational Psychology*, 26(2):139.

Hotelling, H. (1936). Relations between two sets of variates. *Biometrika*, 28(3/4):321–377.

Hull, J. (1994). A database for handwritten text recognition research. *IEEE Transactions on Pattern Analysis and Machine Intelligence*, 16(5):550–554.

Johnson, R. and Wichern, D. (2007). *Applied Multivariate Statistical Analysis*. Pearson Prentice Hall.

Kim, K. and Oh, H.-S. (2024). Principal component analysis in the graph frequency domain. *arXiv preprint arXiv:2410.08422*.

Kim, K. and Oh, H.-S. (2025a). Cross-spectral analysis of bivariate graph signals. *IEEE Transactions on Pattern Analysis and Machine Intelligence*, 47(12):11141–11151.

Kim, K. and Oh, H.-S. (2025b). Graph frequency-domain factor modeling. *IEEE Transactions on Pattern Analysis and Machine Intelligence*, pages 1–13.

Kuylen, A. A. and Verhallen, T. M. (1981). The use of canonical analysis. *Journal of Economic Psychology*, 1(3):217–237.

Leus, G., Marques, A. G., Moura, J. M., Ortega, A., and Shuman, D. I. (2023). Graph signal processing: History, development, impact, and outlook. *IEEE Signal Processing Magazine*, 40(4):49–60.

Marques, A. G., Segarra, S., Leus, G., and Ribeiro, A. (2017). Stationary graph processes and spectral estimation. *IEEE Transactions on Signal Processing*, 65(22):5911–5926.

Mazuruse, P. (2014). Canonical correlation analysis: Macroeconomic variables versus stock returns. *Journal of Financial Economic Policy*, 6(2):179–196.

Mihalik, A., Chapman, J., Adams, R. A., Winter, N. R., Ferreira, F. S., Shawe-Taylor, J., Mourão-Miranda, J., Initiative, A. D. N., et al. (2022). Canonical correlation analysis and partial least squares for identifying brain–behavior associations: A tutorial and a comparative study. *Biological Psychiatry: Cognitive Neuroscience and Neuroimaging*, 7(11):1055–1067.

Ortega, A., Frossard, P., Kovačević, J., Moura, J. M., and Vandergheynst, P. (2018). Graph signal processing: Overview, challenges, and applications. *Proceedings of the IEEE*, 106(5):808–828.

Park, H., Bai, S., Ye, Z., Lee, H., Ma, T., and Chen, S. (2025). Graph canonical correlation analysis. *arXiv preprint arXiv:2502.01780*.

Perraudin, N. and Vandergheynst, P. (2017). Stationary signal processing on graphs. *IEEE Transactions on Signal Processing*, 65(13):3462–3477.

Sandryhaila, A. and Moura, J. M. (2013). Discrete signal processing on graphs. *IEEE Transactions on Signal Processing*, 61(7):1644–1656.

Sandryhaila, A. and Moura, J. M. (2014). Discrete signal processing on graphs: Frequency analysis. *IEEE Transactions on Signal Processing*, 62(12):3042–3054.

Segarra, S., Chepuri, S. P., Marques, A. G., and Leus, G. (2018). Statistical graph signal processing: Stationarity and spectral estimation. In Djurić, P. M. and Richard, C., editors, *Cooperative and Graph Signal Processing*, pages 325–347. Elsevier.

Shuman, D. I., Narang, S. K., Frossard, P., Ortega, A., and Vandergheynst, P. (2013). The emerging field of signal processing on graphs: Extending high-dimensional data analysis to networks and other irregular domains. *IEEE Signal Processing Magazine*, 30(3):83–98.

Singh, R., Chakraborty, A., and Manoj, B. (2016). Graph fourier transform based on directed Laplacian. In *2016 International Conference on Signal Processing and Communications (SPCOM)*, pages 1–5. IEEE.

Thompson, B. (1984). *Canonical Correlation Analysis: Uses and Interpretation*. SAGE Publications.

Tremblay, N., Gonçalves, P., and Borgnat, P. (2018). Design of graph filters and filterbanks. In *Cooperative and Graph Signal Processing*, pages 299–324. Elsevier.

Urtio, V., Monteiro, J. M., Kandola, J., Shawe-Taylor, J., Fernandez-Reyes, D., and Rousu, J. (2017). A tutorial on canonical correlation methods. *ACM Computing Surveys (CSUR)*, 50(6):1–33.

Wróbel, S., Turek, C., Stępień, E., and Piwowar, M. (2024). Data integration through canonical correlation analysis and its application to OMICs research. *Journal of Biomedical Informatics*, 151:104575.

Yang, X., Liu, W., Liu, W., and Tao, D. (2019). A survey on canonical correlation analysis. *IEEE Transactions on Knowledge and Data Engineering*, 33(6):2349–2368.

Yang, X., Liu, W., Tao, D., and Cheng, J. (2017). Canonical correlation analysis networks for two-view image recognition. *Information Sciences*, 385-386:338–352.

Yuan, Y.-H. and Sun, Q.-S. (2014). Graph regularized multiset canonical correlations with applications to joint feature extraction. *Pattern Recognition*, 47(12):3907–3919.

Zhuang, X., Yang, Z., and Cordes, D. (2020). A technical review of canonical correlation analysis for neuroscience applications. *Human Brain Mapping*, 41(13):3807–3833.